Synthesis, characterization of Ag-doped CdS-WO_2 nanocomposite and effects of photocatalytic degradation in RhB under visible light irradiation

G. Roshini
SSN College of Engineering, Chennai.
V. Sathish (sathishv@ssn.edu.in)
SSN College of Engineering, Chennai. https://orcid.org/0000-0001-8964-5777
S. Manigandan
SSN College of Engineering, Chennai.
A. Tamilarasi
SSN College of Engineering, Chennai.
E. Priyanka
SSN College of Engineering, Chennai.

Research Article

Keywords: Ag/CdS-WO2, Rh B, Photocatalyst, Visible light irradiation, Degradation

Posted Date: January 5th, 2022

DOI: https://doi.org/10.21203/rs.3.rs-1228443/v1

Abstract

In this paper, the highly stable Ag/CdS-WO_2 nanocomposite was fabricated by a facile and capping agent-free hydrothermal technique. The fabricated Ag doped CdS-WO_2 nanocomposite were characterized by powder X-ray diffraction (XRD), Fourier transform infrared (FT-IR) spectroscopy and UV-vis diffuse reflectance (DRS) spectroscopy. The photocatalytic performance of synthesized photocatalysts was evaluated for the photodegradation of rhodamine B (Rh B) under visible light irradiation (VLI). The parameters used for the optimization of the photocatalyst were pH, catalyst dose, oxidant dose, and irradiation time. Based on this, a possible reaction mechanism for the enhancement of photocatalytic activity of Ag/CdS-WO_2 has been proposed. Hence, we have a tendency to believe it might be a promising material that may be used for the photodegradation of organic pollutants present in wastewater.

1. Introduction

Water is extremely crucial in our environment for the regular weather and the co-evolution of life on Earth. Almost all of the water on the planet is saline, making it unfit for drinking and irrigation. Only 0.77% occurs as liquid fresh water and its distribution are very in homogeneous [1]. Drinking water should be free of pathogenic germs and contamination by toxic compounds like pesticides and industrial chemicals. Clean and fresh drinking water is essential to human and other life [2]. Water pollution is the contamination of water bodies, usually as a result of industrial wastes. For example, releasing inadequately treated wastewater into natural water bodies can lead to degradation of aquatic ecosystems. The waste bearing water, or effluent, and discharged into streams, lakes, or oceans, which in turn dispersed in the pollutants. Textile dyes and other industrial dyes are very easily mixed with fresh water from several industries [3]. Besides, these dyes can be considered as major water pollutants owing to their contained highly toxic organic compounds. In the current year it is estimated that some 30,000 million liters of pollutants are entering our river systems every day, 10,000 million liters from industrial units alone [4]. Synthetic azo dyes are among common environmental pollutants which are used in various 73 industries including textiles, papers, plastics, pharmaceuticals and cosmetic [5].

Advanced oxidation processes in a broad sense, are a set of chemical treatment procedures designed to remove organic and sometimes inorganic materials in water and waste water by oxidation through reactions with hydroxyl radicals (·OH) [6]. In real-world applications of wastewater treatment, however, this term usually refers more specifically to a subset of such chemical processes that employ ozone (O_3), hydrogen peroxide (H_2O_2) and/or UV light. Photocatalysis is the term can be generally used to describe a process in which light is used to activate a substance [7]. Photocatalysis promises a solution to challenges associated with the intermittent nature of sunlight which is considered as renewable and ultimate energy source to power activities on Earth [8]. Homogeneous photocatalysis refers to catalytic reactions in which both the reactants and the catalyst comprises only one phase and the photochemical process takes place in a homogeneous solution. There are 3 types of homogeneous photocatalysis are

UV/H_2O_2, UV/O_3 and $UV/O_3/H_2O_2$ system. In Heterogeneous photocatalysis, UV/Semiconductor has most common are transition metal oxides and semiconductors, which have unique characteristics. Semiconductor photocatalysis has been gained great attention as a green approach for complete removal of organic pollutants using freely obtainable solar energy source without discharge any secondary pollution [9].

Titanium dioxide (TiO_2) has been widely used as a photocatalyst in many environmental and energy applications due to its efficient photoactivity, high stability, low cost, and safety to the environment and humans [10]. When used in water treatment applications, $TiOS_2$ has a poor affinity toward organic pollutants, especially hydrophobic organic pollutants. Cadmium sulfide, a visible-light responsive photocatalyst with a band gap of 2.4 eV, is one of the most prominent semiconductor photocatalysts [11]. In this study, the influences of Ag/CdS-WO_2 Nano composite on the photodegradation of organic pollutant in aqueous solution were investigated. Hence, the objectives of this work are, (i) To synthesis Ag doped CdS-WO_2 ternary nanocomposite via hydrothermal method. And prepare the photocatalyst with suitable semiconductor material. (ii) To characterized the synthesized material by using X-ray diffraction (XRD) and Fourier transform infrared (FT-IR), UV-vis diffuse reflectance spectra (DRS). (iii) To study the photocatalytic performance of the pure CdS, pure WO_2, CdS-WO_2 and Ag/CdS-WO_2 photocatalyst by their ability in the photocatalytic degradation of Rhodamine-B (RhB) as a target textile pollutant under visible-light irradiation. (iv) To study the optimization of different process parameters and effects like pH, catalyst concentration, concentration of oxidants (persulphate), and irradiation time. (v) Finally, To propose a possible reaction mechanism related to the enhanced photocatalytic degradation of Ag/CdS-WO_2 photocatalyst.

2. Materials And Methods

2.1. Chemicals

Cetyl trimethyl ammonium bromide (CTAB), sodium sulfide (Na_2S), ethanol (EtOH) and sodium hydroxide (NaOH), cadmium nitrate [Cd $(NO_3)_3$], were purchased from SDFCL, India. Silver nitrate ($AgNO_3$, 99%) was obtained from Sigma-Aldrich. Tungstic acid (H_2WO_4, 99%) and Hydrogen peroxide (30% w/v of H_2O_2) was obtained from Nice chemicals, India. Rhodamine B (98%) was purchased from UNI-CHEM. Double distilled-water (ddH_2O) water was used throughout the experiments, prepared by typical laboratory distillation unit. All chemicals were of analytical grade and were used without any further purification.

2.2. Synthesis of CdS

In a typical procedure, 50 mL of 1 M cadmium nitrate, 25 mL of distilled water, 25 mL of ethanol and 0.34 g CTAB were mixed in a beaker. To this solution, 50 mL of 1M Na_2S, 25 mL ethanol and 25 mL distilled water were added with vigorous stirring. Following this 20 mL of 2M NaOH was added with vigorous stirring which gives a light yellow precipitate. This mixture was transferred to a 250 mL Teflon-lined stainless steel autoclave, followed by heating at 100°C for 2 h [12]. Following this, it was cooled to room

temperature and the residue obtained was separated by centrifugation, washed several times with distilled water, ethanol and then dried in oven at 40°C, to get the resulting is the yellow coloured cadmium sulphide.

2.3. Synthesis of WO_2

2 g of tungstic acid and 0.895 g of CTAB were dissolved in 50 mL of distilled water. Then, the solution was transferred into a Teflon-lined autoclave. The hydrothermal reaction was carried out in hot air oven at 120 ℃ for 12 h and then it allowed cooling at room temperature. The obtained yellow color precipitate was collected, washed with deionized water and ethanol several times to remove impurities, and dried in hot air oven at 60 ℃ for 6 h [13].

2.4. Synthesis of CdS-WO_2

For preparing CdS-WO_2 composite, 0.2 g of the above prepared WO_2 was dissolved in 80 ml ethanol to make a non-homogenous mixture and sonicated for half an hour. 1 g of CdS nanoparticles which was synthesized by the simple hydrothermal method was mixed in 100 ml of water and sonicated for half an hour. The above prepared WO_2 suspension was added into the CdS mixture and sonicated for 30 more minutes. The resulting mixture was filled into a Teflon-lined stainless-steel autoclave at 200°C for 12 h. The obtained precipitates were filtered and rinsed many times with distilled water and ethanol. Finally, the formed product was dried at 60°C for 12 h [14].

2.5. Synthesis of Ag/CdS-WO_2 Nano composite

Ag/CdS-WO_2 (5 wt %) Nano composite was made by adding 0.5 g of CdS-WO_2 into 40 ml ethylene glycol solution with constant stirring for 20 min. afterward, the mixture was heated for 2 h at 180°C; then 0.025 g (2.7%) $AgNO_3$ was added with constant stirring for 30 min. The resulting mixture was cooled at room temperature, washed by ethanol three times, and finally dried at 60°C for 3 h [15].

Figure 1 shows the Schematic methodology of synthesis of Ag/CdSWO_2 nanocomposite.

2.6. Characterization of photocatalysts

X-ray diffraction (XRD) patterns of the synthesized photocatalysts were recorded using a X-ray diffractometer (Mini Flex II, Japan) with Cu Kα radiation (l ¼ 0.154 nm) at a scan speed of 3°/min. The phase purity was ascertained using X-ray diffraction. The Fourier transform infrared (FT-IR) spectra were recorded to study the interaction among CdS and WO_2 with a wavenumber ranging from 4000–400 cm^{-1} using a JASCO 460 plus FT-IR instrument. UV-vis diffuse reflectance spectra (DRS) were recorded using a Shimadzu 2100 spectrophotometer in the range of 200–800 nm.

2.7. Photocatalytic degradation studies

The photocatalytic activity of the as-synthesized photocatalyst was evaluated by the photo degradation of RhB under visible-light irradiation using a photocatalysis chamber. A 250W tungsten halogen lamp

was employed as a source of visible-irradiation. A 75 mL of the RhB dye solution to achieve a catalyst concentration of 1.0 g/L. Prior to light irradiation, the suspension was magnetically stirred in the dark for 60 min to reach an adsorption-desorption equilibrium at room temperature [16]. During irradiation, 4 mL of aliquots was collected at regular time interval and then the photocatalyst was removed by centrifugation. The characteristic absorption wavelength of 554 nm for RhB was followed by using a UV-visible spectrometer (Jasco-630) Japan.

3. Results And Discussions

3.1. XRD studies

The crystalline phase and the purity of the as-synthesized bare CdS, bare WO_2, CdS-WO_2, and Ag/CdS-WO_2 nanocomposites were examined by XRD results are depicted in Fig. 2. The phase and structure of CdS semiconductor were investigated by XRD technique. The powder XRD pattern of CdS nanoparticles was well matched with the hexagonal phase structure (JCPDS File no. 10–0454). The diffraction peaks appeared at 20.93°, 35.04°, 43.52°, 48.8°, 52.02°, 55.97°, and 61.09° corresponding to the (101), (102), (110), (103), (201), (004), and (104) planes, respectively. No impurity peak was observed. Furthermore, peak broadening was observed implying either the amorphous nature of the compound or the nano crystalline behavior of the sample [12]. The XRD pattern of pure WO_2 displayed monoclinic crystal structure corresponding to the (002), (200), (120), (112), and (222), diffraction at 2θ = 21.02°, 24.47°, 26.85°, 27.94° and,42.03°, (JCPDS no. 43-1035). The XRD patterns of Ag/CdS-WO_2 Nano composites contain only monoclinic WO_2 peaks with no other peaks of CdS. Due to less available content of CdS nanoparticles may be the reason for absence of CdS peaks. However, the peak intensity of WO_2 increased with an ascending amount of CdS in the Ag/CdS-WO_2 Nano composites [17].

3.2. FT-IR spectroscopy studies

The purity and functional group composition of the synthesized CdS, WO_2, CdS–WO_2 and Ag/CdS-WO_2 were investigated by using a Fourier transform infrared (FT-IR) spectroscopy in the region of 400–4000 cm^{-1} [18]. The FT-IR spectrum of CdS, WO_2, CdS–WO_2 and Ag/CdS-WO_2 Nano composites is shown in Fig. 3. In the FT-IR spectrum of pure CdS, the absorption peaks at 541 cm^{-1} and 1032 cm^{-1} are assigned to Cd–S stretching modes and bending modes of H–O–H of absorbed water molecules in sulphide products [19]. In the spectrum of WO_2, the sharp peak at 542 cm^{-1} corresponds to the stretching vibration modes of O–W–O bonds. The absorption peaks at 1434 and 1654 cm^{-1} corresponds to the asymmetric and bending vibration of water on the surface of the WO_2 in the sample [20]. The characteristic broad peak at 3453 cm^{-1} may be due to the stretching frequency of the O-H stretching [21]. The sharp absorption peaks at 541 and 1038 cm^{-1} due to the Cd–S stretching modes and broad peak at 3527 cm^{-1} is for O-H stretching. The new distinct peak observed at 1026 cm^{-1} for the Ag doped CdS-WO_2

photocatalysts corresponds to asymmetric valence S=O vibration [22]. Thus, the FT-IR results clearly indicate the existence of Ag in the CdS-WO_2 photocatalyst.

3.3. Optical absorption studies

The light absorption properties of CdS, WO_2, CdS-WO_2 and Ag/CdS-WO_2 photocatalysts were investigated by UV-vis diffuse reflectance spectroscopy and the spectral characteristics are displayed in Fig. 4. The absorption photo peaks for the synthesized CdS, WO_2, CdS-WO_2 and Ag/CdS-WO_2 are found to be at 423, 510, 525 and 485 nm, respectively and the corresponding calculated band energy gap values are 2.93, 2.43, 2.36 and 2.55 eV, respectively. It should be noted that the visible light absorption capacity is increased for the CdS with the introduction of WO_2. As seen from the Figure 4 the variation of CdS photocatalyst exhibited a limited photocatalytic performance towards degradation of RhB with an efficiency of 82.5, 93.2, 95.0 and 96.5% after 90 min irradiation, respectively [23–25]. The degradation of RhB dye is due to the synergistic effect of both adsorption and photo catalysis. It should be noted that a significant improvement of RhB degradation can be found in the presence of both catalyst and light.

3.4. Photocatalytic degradation studies

3.4.1. Effect of pH

The photocatalytic activities of prepared catalysts were investigated at different pH values (3–9). At increased pH (i.e., > 8) the degradation of rhodamine B decreased because of the formation of aromatic hydroxylated species that appears in the form of anions and competes with the adsorption of dye molecules which results in a decrease in degradation efficiency. Therefore the condition of optimum pH is mandatory for avoiding the wastage of excess quantity of catalyst; furthermore, it helps in maximum assimilation of visible light for enhanced photodegradation [26]. In Fig. 5 graph (a) shows the variation of pH trend of catalysts. CdS shows maximum degradation of 65% at neutral pH = 7. WO_2 shows better degradation because of the availability of the enhanced active sites on 75% at neutral pH (i.e., 7). Similarly, the CdS-WO_2 catalyst showed maximum degradation of 76% at neutral pH = 7. The ultimate degradation of 90% by Ag/CdS-WO_2 was even more than the other two catalysts. As a result of the loading of Ag on CdS-WO_2 surface, the possibilities of dye molecules adsorption on the surface of the catalyst enhance due to the increased availability of active sites.

3.4.2. Effect of catalyst concentration

For the optimization of catalyst dose in degrading rhodamine B dye, the amount of CdS, WO_2, CdS-WO_2, and Ag/CdS-WO_2 was varied from 10 to 90 mg/100 ml. Figure 6 shows that by increasing catalyst dose the degradation intensifies due to the availability of enhanced active sites. The trend remained up to a certain limit (i.e., Ag/CdS-WO_2 = 75, 150, 225, 300 mg/100 ml) above which the results showed reduced

degradation of rhodamine B due to the formation of agglomerates [27]. Hence the maximum degradation is obtained at the above-mentioned catalyst loading of specific catalysts.

3.4.3. Effect of oxidant concentration

In order to examine the role of $S_2O_8^{2-}$, experiments of the photocatalytic degradation of RhB employing different initial concentrations of the oxidant in the range of 3 to 13 mM. The influence of oxidant dose for dye degradation was observed for three different catalysts CdS, WO_2, CdS-WO_2, and Ag/CdS-WO_2. And the results are depicted in Figure 7. It is evident that the degradation increased with increase in concentration of $S_2O_8^{2-}$ under the experimental conditions studied. The percentage of decolourization is increased with the increase in of the initial per sulfate concentration 43.41, 72.40, 74.40% and 79.32%. The enhancement can be attributed to the ability of persulfate to act as an electron acceptor [28].

Due to its high potential (2.6 eV) sulphate radicals which is a powerful oxidant that can able to participate in RhB degradation. This is the reason for decrease of rate [29].

$$S_2O_8^{2-} + e_{CB}^{-} \rightarrow SO_4^{2-} + SO_4^{2-}$$

$$SO_4^{2-} + H_2O \rightarrow SO_4^{2-} + HO\cdot + H^+$$

$$SO_4^{2-} + h^+ \rightarrow SO_4^{2-}$$

$$SO_4^{2-} + HO\cdot \rightarrow SO_4^{2-} + HO^-$$

3.4.4. Effect of irradiation time

Optimization of time can be attained by keeping the above three parameters pH, oxidant dose, and amount of catalyst constant and time was altered (10–90 min). The degradation was monitored for four different catalysts such as CdS, WO_2, CdS-WO_2, and Ag/CdS-WO_2. After complete time intervals, the catalysts were taken from the reaction mixture and their absorbances were checked using a spectrophotometer. Fig. 8 shows the UV–visible spectra of RhB irradiated with visible light at different time intervals in the presence of the Ag/CdS-WO_2 photocatalyst. The obtained results are presented in terms of percentage degradation in Fig. 9. It is clear from the results that, percentage degradation increases successively over time. After 70 min the highest efficiencies were recorded with the catalysts, therefore 70 min was selected as the optimum time from the best efficiency of respective catalysts under corresponding optimized conditions.

3.5. Reaction Kinetics

For the quantitative study of RhB degradation, the pseudo first-order kinetic model was employed to analyze the experimental data. For photocatalytic experiments, the equation is specifically designed when we take the concentration of the pollutant in the mill molar range.

$$\ln \frac{C_{\varvec{o}}}{\varvec{C}} = -\varvec{k}\varvec{t}$$

Where C_o = is the initial concentration, C = is the final concentration of RhB at time t. The plot of ln (C_o/C) versus time gives a linear response, and the value of k can be analyzed from the slope of pseudo first-order reaction and displayed in figure 10. The results clearly state that the K (rate constant) value of different dye concentrations like 75, 150 and 225 g/L of Ag/CdS-WO_2 for the degradation of RhB. Results shows the 75 g/L of Ag/CdS-WO_2 was higher than 150 and 225 g/L of Ag/CdS-WO_2 which reveals the fact that the combination of both of the catalysts further enhances the degradation ability as compared to the individual catalyst. Finally, Ag/CdS-WO_2 was the novel nanocomposite with unique characteristics among other composites.

3.6. Photocatalytic degradation mechanism

The electron in the valence band (VB) is excited to the conduction band by visible light absorption and the generation of hole (h^+) in the valence band [30]. The electrons and holes transfer to the surface of the CdS and react with the molecular oxygen (O_2) and H_2O to generate the superoxide radical anion ($\cdot O_2^-$) and hydroxyl radical (·OH), which act as the active center and strong oxidizing agent for the photo catalytic activity [23, 24, 28, 29]. The degradation of RhB under the irradiation of the stimulated visible light depends on two reactions like de-ethylation and decomposition of chromophore structure of the RhB. These processes can be characterized by the shift of the maximum absorption band ($\lambda_{.max}$) and change in the absorption maximum C_{max} /C^o_{max} respectively [31]. Thus the process of producing photo excited e^- can be used to generate more $\cdot O_2^-$ from O_2, subsequently accelerating reaction with organic dyes. At the same time, holes in the valence band (h^+) also have certain degrading ability to RhB. Combined with two active species $\cdot O_2^-$ and h^+, photo catalyst can degrade organic dyes in a short time [32].

Thus, the promising reaction mechanism involving RhB dye photodegradation can be given as follows:

Ag/CdS-WO_2 + hv → e^- + h^+

e^- + O_2 → $\cdot O_2^-$

$\cdot O_2^-$ + 2H_2O + e^- → 2·OH + $2HO^-$

$\cdot O_2^-$ + RhB dye → products

h^+ + RhB dye → products

Based on the above calculations, the probable photocatalytic degradation mechanism in the presence of nanocomposite photocatalyst is shown schematically in the Fig. 11,

4. Conclusions

The highly stable Ag/CdS-WO_2 nanocomposite was fabricated by a facile and capping agent-free hydrothermal technique. The effect of phtocatalyst amounts; initial dye concentration and $K_2S_2O_8$ become studied. The degradation of RhB follows pseudo-first order kinetics in all cases. The results of this study clearly showed that the presence of oxidants could have an important impact on the photocatalytic degradation efficiency of the parent compound as well as on the transformation rate of the organic intermediates. The degradation efficiency was found to be strongly influenced by the concentration levels of the $S_2O_8^{2-}$. The initial concentration of $S_2O_8^{2-}$ showed an obviously positive effect on the degradation process appreciably enhancing photodegradation efficiency of RhB. $S_2O_8^{2-}$ showed the most pronounced effect on the decomposition of RhB. The addition of a minute amount of oxidant is an inexpensive way to greatly improve the degradation rate of a photocatalyst. The novel composite Ag/CdS-WO_2 has valuable applications in pollutant degradation.

Declarations

Competing interests: The authors declare no competing interests.

References

1. Gleick, P.H., 1993. *Water in crisis* (Vol. 100). New York: Oxford University Press.
2. Gatidou, G., Arvaniti, O.S. and Stasinakis, A.S., 2019. Review on the occurrence and fate of microplastics in Sewage Treatment Plants. *Journal of hazardous materials*, *367*, pp.504–512. https://doi.org/10.1016/j.jhazmat.2018.12.081
3. Goel, P.K., 2006. *Water Pollution-Causes, Effects and Control. New Delhi: New Age International* (p. 179). ISBN 978-81-224-1839-2.
4. Verma, A.K., Dash, R.R. and Bhunia, P., 2012. A review on chemical coagulation/flocculation technologies for removal of colour from textile wastewaters. *Journal of environmental management*, *93*(1), pp.154-168. https://doi.org/101016/j.jenvam.2011.09.012.
5. Kumar, P., Prasad, B., Mishra, I.M. and Chand, S., 2007. Catalytic thermal treatment of desizing wastewaters. *Journal of hazardous materials*, *149*(1), pp.26–34. https://doi.org/10.1016/j.jhazmat.2007.03.051
6. Spellman, F.R., 2015. *Reverse osmosis: a guide for the nonengineering professional*. CRC Press.
7. Bruner, L. and Kozak, J., 1911. Information on the photocatalysis I the light reaction in uranium salt plus oxalic acid mixtures. *Z. Elktrochem. Angew. Phys. Chem*, *17*(9), pp.354–360.
8. Linsebigler, A.L., Lu, G. and Yates Jr, J.T., 1995. Photocatalysis on TiO2 surfaces: principles, mechanisms, and selected results. *Chemical reviews*, *95*(3), pp.735–758. https://doi.org/10.1021/cr00035a013

9. Daneshvar, N., Salari, D. and Khataee, A.R., 2004. Photocatalytic degradation of azo dye acid red 14 in water on ZnO as an alternative catalyst to TiO2. *Journal of photochemistry and photobiology A: chemistry*, *162*(2-3), pp.317–322. https://doi.org/10.1016/S1010-6030(03)00378-2
10. Borges, M.E., Sierra, M., Cuevas, E., García, R.D. and Esparza, P., 2016. Photocatalysis with solar energy: Sunlight-responsive photocatalyst based on TiO2 loaded on a natural material for wastewater treatment. *Solar Energy*, *135*, pp.527–535. https://doi.org/10.1016/j.solener.2016.06.022
11. Wang, Q., Lian, J., Ma, Q., Bai, Y., Tong, J., Zhong, J., Wang, R., Huang, H. and Su, B., 2015. Photodegradation of Rhodamine B over a novel photocatalyst of feather keratin decorated CdS under visible light irradiation. *New Journal of Chemistry*, *39*(9), pp.7112–7119. https://doi.org/10.1039/c5nj00987a
12. Al Balushi, B.S., Al Marzouqi, F., Al Wahaibi, B., Kuvarega, A.T., Al Kindy, S.M., Kim, Y. and Selvaraj, R., 2018. Hydrothermal synthesis of CdS sub-microspheres for photocatalytic degradation of pharmaceuticals. *Applied Surface Science*, *457*, pp.559–565. https://doi.org/10.1016/j.apsusc.2018.06.286
13. Xing, L.L., Deng, P., He, B., Nie, Y.X., Wu, X.L., Yuan, S., Cui, C.X. and Xue, X.Y., 2014. Assembly of FeWO4-SnO2 core-shell nanorods and their high reversible capacity as lithium-ion battery anodes. *Electrochimica Acta*, *118*, pp.45–50. https://doi.org/10.1016/j.electacta.2013.11.178
14. Gao, Q. and Liu, Z., 2017. FeWO4 nanorods with excellent UV–Visible light photocatalysis. *Progress in Natural Science: Materials International*, *27*(5), pp.556–560. https://doi.org/10.1016/j.pnsc.2017.08.016
15. Ojha, D.P., Karki, H.P., Song, J.H. and Kim, H.J., 2019. Amine-assisted synthesis of FeWO4 nanorodg-C3N4 for enhanced visible light-driven Z-scheme photocatalysis. *Composites Part B: Engineering*, *160*, pp.277–284. https://doi.org/10.1016/j.compositesb.2018.10.039
16. Li, Z. and Du, Y., 2003. Biomimic synthesis of CdS nanoparticles with enhanced luminescence. *Materials Letters*, *57*(16-17), pp.2480–2484. https://doi.org/10.1016/S0167-577X(02)01297-1
17. Ganesh, R.S., Durgadevi, E., Navaneethan, M., Sharma, S.K., Binitha, H.S., Ponnusamy, S., Muthamizhchelvan, C. and Hayakawa, Y., 2017. Visible light induced photocatalytic degradation of methylene blue and rhodamine B from the catalyst of CdS nanowire. *Chemical Physics Letters*, *684*, pp.126–134. https://doi.org/10.1016/j.cplett.2017.06.021
18. Senasu, T., Hemavibool, K. and Nanan, S., 2018. Hydrothermally grown CdS nanoparticles for photodegradation of anionic azo dyes under UV-visible light irradiation. *RSC advances*, *8*(40), pp.22592–22605. https://doi.org/10.1039/c8ra02061b
19. Saranya, M., Santhosh, C., Ramachandran, R. and Nirmala Grace, A., 2014. Growth of CuS nanostructures by hydrothermal route and its optical properties. *Journal of Nanotechnology*, *2014*. https://doi.org/10.1155/2014/321571
20. Jiang, Z., Xie, J., Jiang, D., Wei, X. and Chen, M., 2013. Modifiers-assisted formation of nickel nanoparticles and their catalytic application to p-nitrophenol reduction. *CrystEngComm*, *15*(3), pp.560–569. https://doi.org/10.1039/C2CE26398J

21. Sharma, N., Deepa, M., Varshney, P. and Agnihotry, S.A., 2002. FTIR and absorption edge studies on tungsten oxide based precursor materials synthesized by sol–gel technique. *Journal of non-crystalline solids*, *306*(2), pp.129–137. https://doi.org/10.1016/S0022-3093(02)01134-1
22. Andronic, L., Isac, L. and Duta, A., 2011. Photochemical synthesis of copper sulphide/titanium oxide photocatalyst. *Journal of Photochemistry and Photobiology A: Chemistry*, *221*(1), pp.30–37. https://doi.org/10.1016/j.jphotochem.2011.04.018
23. Reza, K.M., Kurny, A.S.W. and Gulshan, F., 2017. Parameters affecting the photocatalytic degradation of dyes using TiO2: a review. *Applied Water Science*, *7*(4), pp.1569–1578. https://doi.org/10.1007/s13201-015-0367-y
24. Yang, S., Huang, Y., Wang, Y., Yang, Y., Xu, M. and Wang, G., 2012. Photocatalytic degradation of Rhodamine B with H3PW12O40/SiO2 sensitized by H2O2. *International Journal of Photoenergy*, *2012*. https://doi.org/10.1155/2012/927132
25. Shen, Q., Xue, J., Mi, A., Jia, H., Liu, X. and Xu, B., 2013. The study on properties of CdS photocatalyst with different ratios of zinc-blende and wurtzite structure. *RSC advances*, *3*(43), pp.20930–20935. https://doi.org/10.1039/c3ra42179a
26. Lee, K.M. and Hamid, S.B.A., 2015. Simple response surface methodology: investigation on advance photocatalytic oxidation of 4-chlorophenoxyacetic acid using UV-active ZnO photocatalyst. *Materials*, *8*(1), pp.339–354. https://doi.org/10.3390/ma8010339
27. Shi, D., Yan, F., Wang, M., Zou, Y., Zheng, T., Zhou, X. and Chen, L., 2015. Rhodamine derivative functionalized chitosan as efficient sensor and adsorbent for mercury (II) detection and removal. *Materials Research Bulletin*, *70*, pp.958–964. https://doi.org/10.1016/j.materresbull.2015.06.046
28. Chen, X., Xue, Z., Yao, Y., Wang, W., Zhu, F. and Hong, C., 2012. Oxidation degradation of rhodamine B in aqueous by treatment system. *International Journal of Photoenergy*, *2012*. https://doi.org/10.1155/2012/754691
29. Liang, C. and Su, H.W., 2009. Identification of sulfate and hydroxyl radicals in thermally activated persulfate. *Industrial & Engineering Chemistry Research*, *48*(11), pp.5558–5562. https://doi.org/10.1021/ie9002848
30. Xie, Y., Zhang, S., Pan, B., Lv, L. and Zhang, W., 2011. Effect of CdS distribution on the photocatalytic performance of resin-CdS nanocomposites. *Chemical engineering journal*, *174*(1), pp.351–356. https://doi.org/10.1016/j.cej.2011.09.006
31. Jiang, R., Zhu, H., Li, X. and Xiao, L., 2009. Visible light photocatalytic decolourization of CI Acid Red 66 by chitosan capped CdS composite nanoparticles. *Chemical Engineering Journal*, *152*(2-3), pp.537–542. https://doi.org/10.1016/j.cej.2009.05.037
32. Chen, F., Jia, D., Cao, Y., Jin, X. and Liu, A., 2015. Facile synthesis of CdS nanorods with enhanced photocatalytic activity. *Ceramics International*, *41*(10), pp.14604–14609. https://doi.org/10.1016/j.ceramint.2015.07.179

Figures

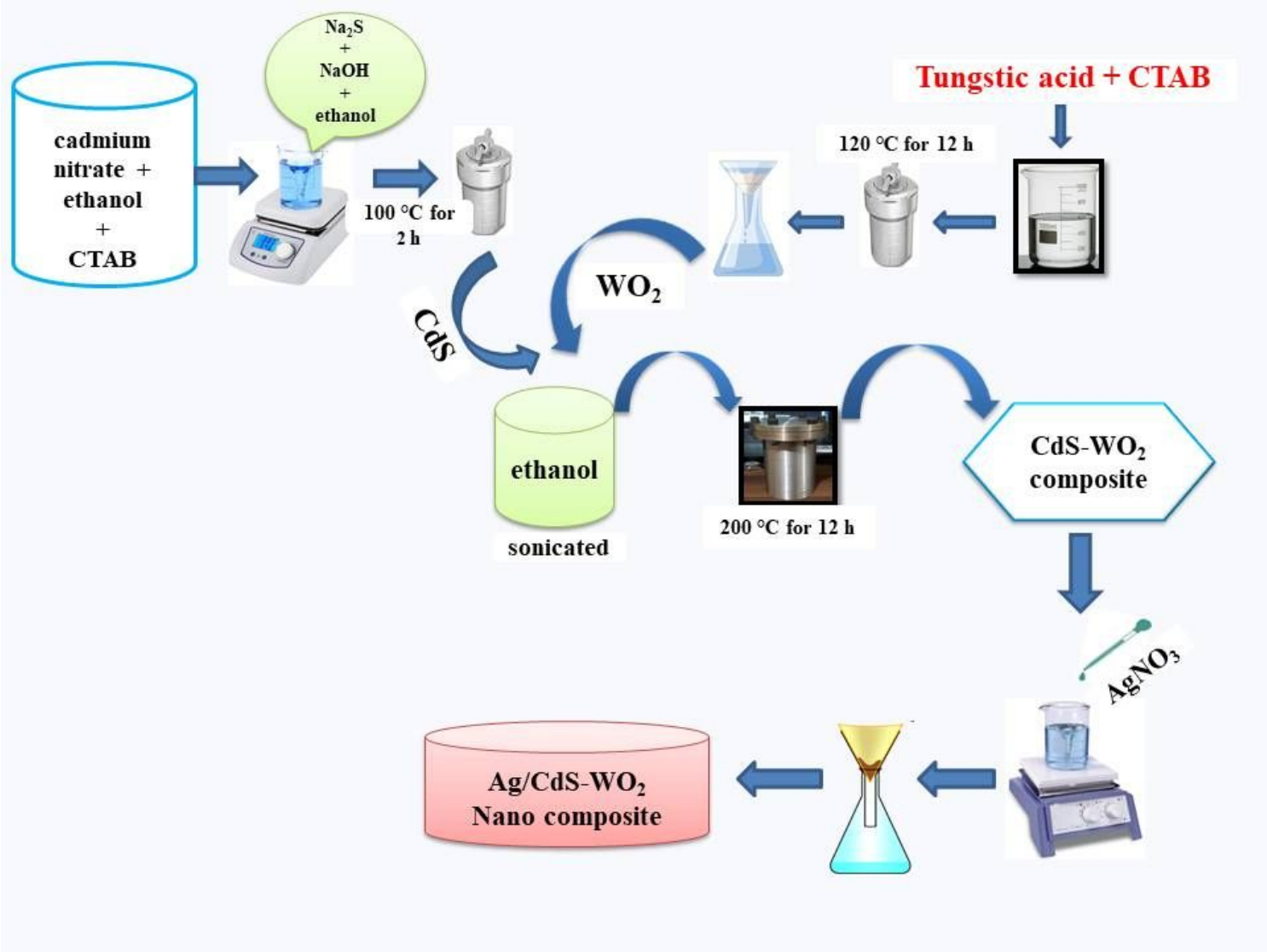

Figure 1

Schematic methodology of synthesis of Ag/CdS-WO_2 nanocomposite

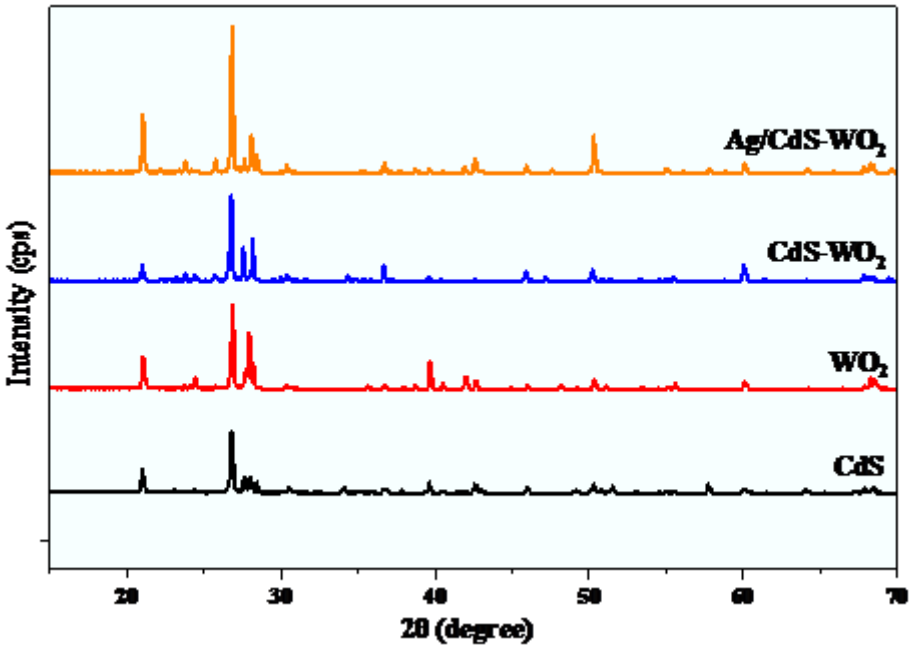

Figure 2

XRD spectrum of (a) CdS, (b) WO_2, (c) CdS-WO_2 and (d) Ag/CdS-WO_2

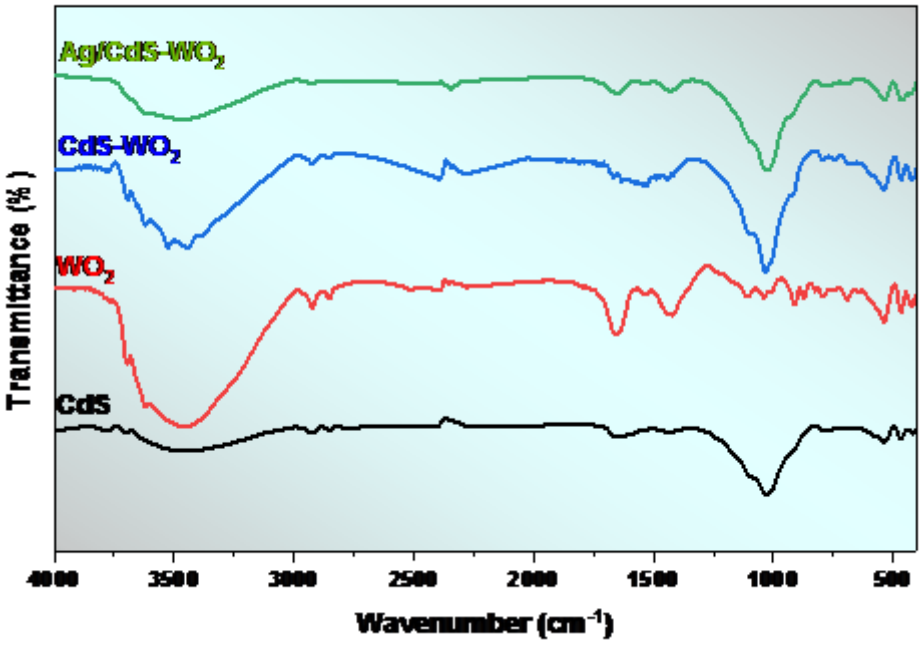

Figure 3

FT-IR spectrum of CdS, WO_2, CdS–WO_2 and Ag/CdS-WO_2 Nanocomposites

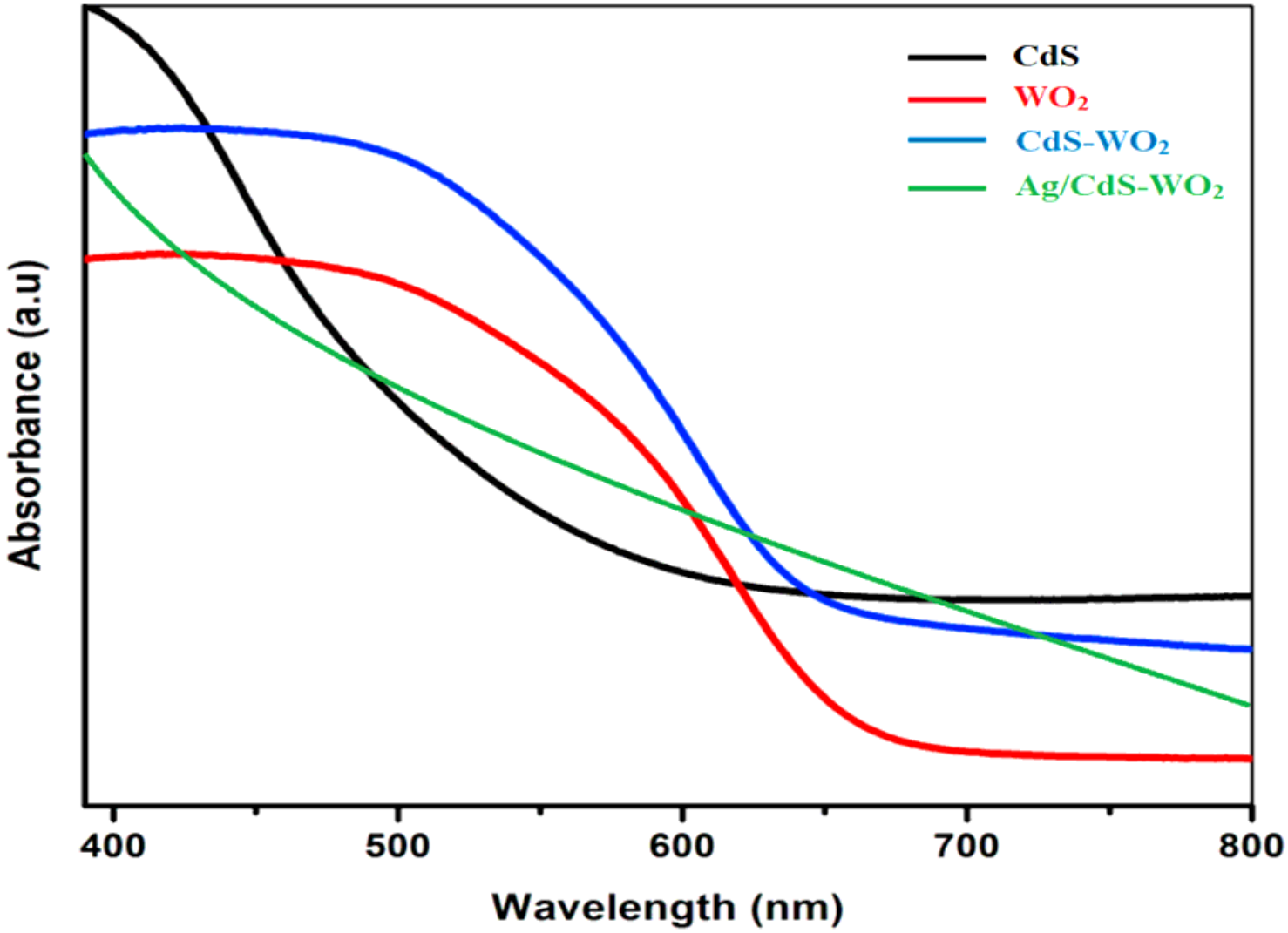

Figure 4

UV-DRS of CdS, WO_2, CdS–WO_2 and Ag/CdS-WO_2 Nanocomposites

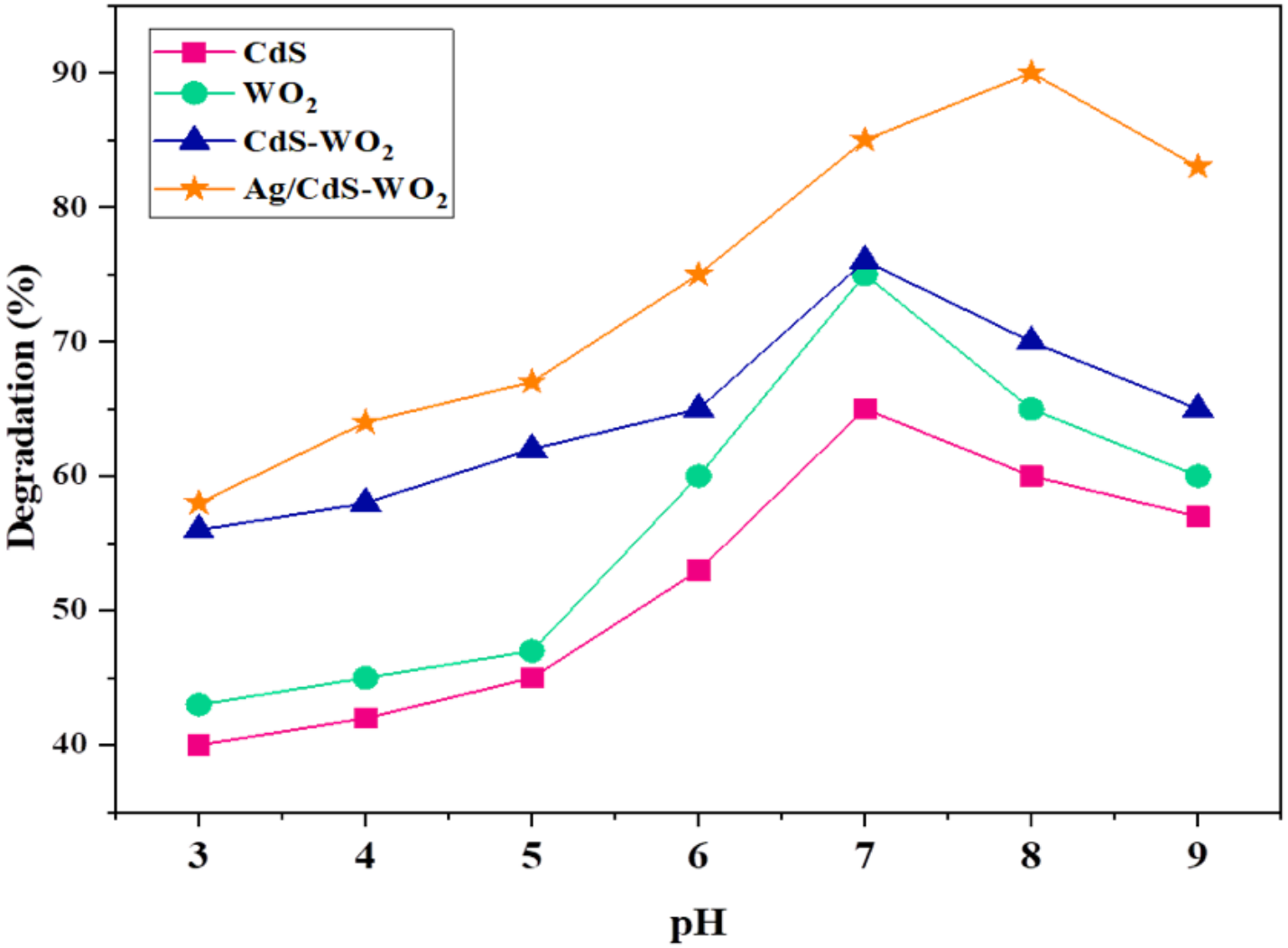

Figure 5

Optimization of reaction parameter of pH using CdS, WO_2, CdS–WO_2 and Ag/CdS-WO_2

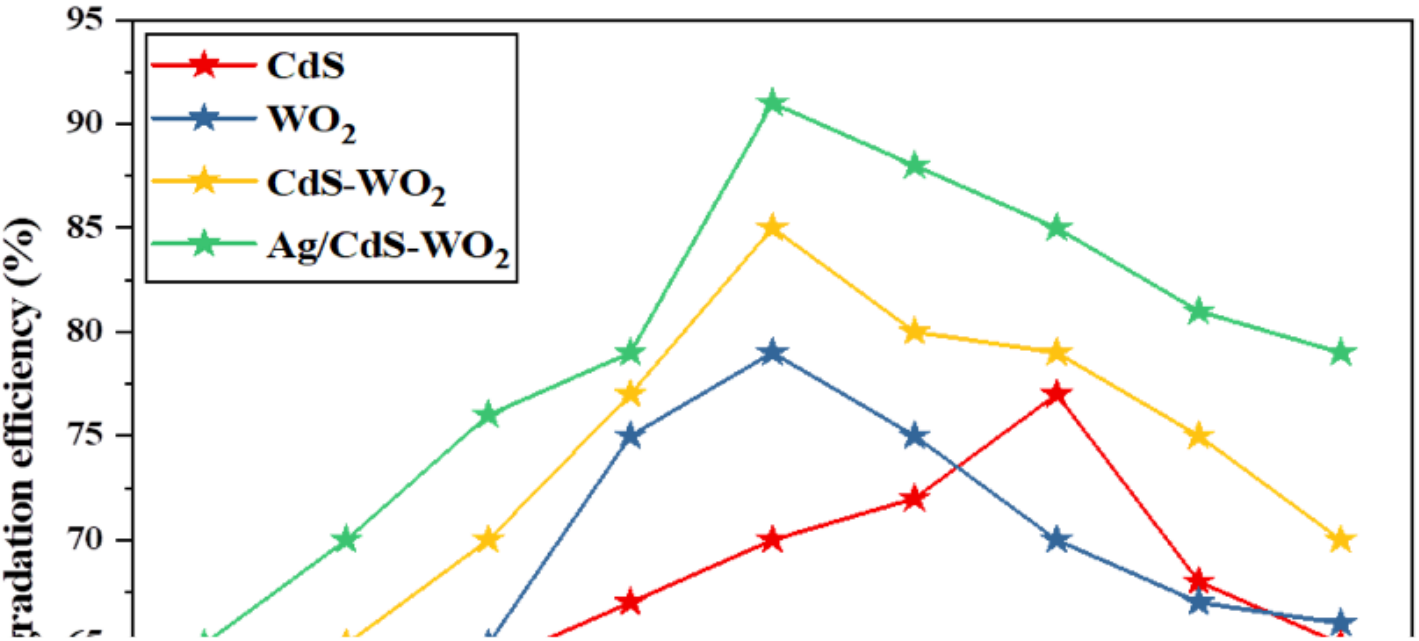

Figure 6

Optimization of reaction parameter of catalyst dose using CdS, WO_2, CdS–WO_2 and Ag/CdS-WO_2

Figure 7

Optimization of reaction parameter of oxidant dose using CdS, WO_2, CdS–WO_2 and Ag/CdS-WO_2

Figure 8

UV–visible spectra of RhB at different time intervals of Ag/CdS-WO_2

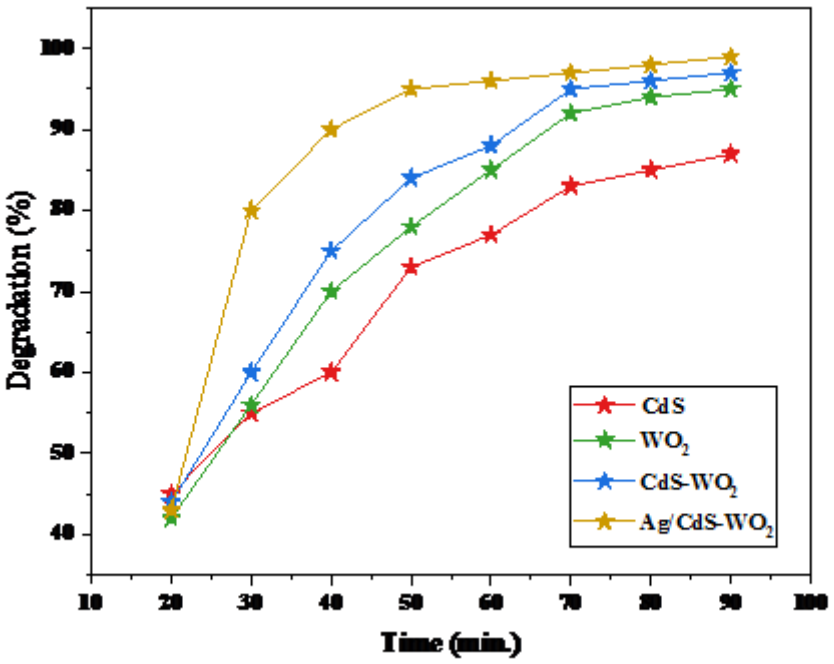

Figure 9

Optimization of reaction parameter of irradiation time using CdS, WO_2, CdS–WO_2 and Ag/CdS-WO_2

Figure 10

Pseudo-first-order kinetic fitted curves of Rh B over Ag/CdS-WO_2 composite

Figure 11

The schematic representation of Ag/CdS-WO_2 nanocomposite photocatalyst towards the degradation of RhB under VLI.